NMR solution conformation of heparin-derived tetrasaccharide

Dmitri MIKHAILOV*, Kevin H. MAYO*‡, Ioncho R. VLAHOV†, Toshihiko TOIDA†, Azra PERVIN† and Robert J. LINHARDT†

*Departments of Biochemistry and Laboratory of Medicine and Pathology, Biomedical Engineering Center, University of Minnesota Medical School, 420 Delaware Street, S.E., Minneapolis, MN 55455, U.S.A., and †Department of Medicinal and Natural Products Chemistry, College of Pharmacy, The University of Iowa, 115 S. Grand Ave., Iowa City, IA 52242, U.S.A

The solution conformation of the homogeneous, heparin-derived tetrasaccharide ΔUA2S(1 → 4)-α-D-GlcN*p*S6S(1 → 4)-α-L-IdoA*p*2S(1 → 4)-α-D-GlcN*p*S6S (residues A, B, C and D respectively, where IdoA is iduronic acid) has been investigated by using ^{1}H- and ^{13}C-NMR. Ring conformations have been defined by *J*-coupling constants and inter-proton nuclear Overhauser effects (NOEs), and the orientation of one ring with respect to the other has been defined by inter-ring NOEs. NOE-based conformational modelling has been done by using the iterative relaxation matrix approach (IRMA), restrained molecular dynamics simulations and energy minimization to refine structures and to distinguish between minor structural differences and equilibria between various ring forms. Both glucosamine residues B and D are in the $^4C_1$ chair conformation. The 6-*O*-sulphate group is oriented in the *gauche–trans* configuration in the D ring, whereas in the B ring the *gauche–gauche* rotomer predominates. Uronate (A) and iduronate (C) residues are mostly represented by $^1H_2$ and $^2S_0$ twisted boat forms, respectively, with small deviations in expected coupling constants and NOEs suggesting minor contributions from other A and C ring conformations.

INTRODUCTION

Heparin is mainly a polydisperse sulphated copolymer of 1 → 4-linked glucosamine and uronic acid residues. Most of the heparin molecule is accounted for by this repeating disaccharide unit that consists primarily of 2-*O*-sulpho-α-L-idopyranosyluronic acid (α-L-IdoA*p*2S) and 2-amino-2-deoxy-di-2,6-sulpho-α-D-glucopyranose (α-D-GlcN*p*S6S) [1,2], although both β-D-glucopyranosyluronic acid and α-L-idopyranosyluronic acid residues are also found. The major repeating sequence, → 4)-α-L-IdoA*p*2S(1 → 4)-α-D-GlcN*p*S6S(1 → , represents at least 85% of heparins from bovine lung and about 75% of those from intestinal mucosa [3]. The remainder of the molecule is made up of residues of 2-amino-2-deoxy-2-acetyl (or sulpho)-α-D-glucopyranose, β-D-glucopyranosyluronic acid and α-L-idopyranosyluronic acid, although their distributions within the polymer, as well as their degree and position of sulphation, have yet to be established unequivocally.

Isolation and chemical composition of the most common tetrasaccharide repeat unit in heparin, UA2S(1 → 4)-α-D-GlcN*p*S6S(1 → 4)-α-L-IdoA*p*2S(1 → 4)-α-D-GlcN*p*S6S, have been reported [4,5]. The chemical structure of this tetrasaccharide is shown in Figure 1 with residues labelled A to D. ^{1}H- and ^{13}C-NMR assignments have been made for this tetrasaccharide unit [6] as well as for various other heparin-derived oligosaccharides [7,8]. However, little is known about the solution conformation of oligosaccharides prepared via heparin depolymerization. In general the overall conformation could be described by a set of glycosidic bond dihedral angles and the orientation of exocyclic groups.

Heparinase depolymerization produces at the non-reducing end a terminal uronate with an unsaturated 4,5 carbon bond. For di- and oligosaccharides that have been studied by NMR [4,9], proton coupling constants for this terminal uronate indicate conformational flexibility. Crystallographic data show that this residue exists in two different forms ($^2H_1$ and $^1H_2$) within the same unit cell, indicating that these are of nearly equal energies [10]. The non-terminal α-L-idopyranosyluronate residue is likewise internally flexible whereas 2-deoxy-2-aminoglucopyranose and β-D-glucopyranosyluronate residues are conformationally rigid in solution [11,12]. Although derivation of the conformation of iduronate-containing polysaccharides and oligosaccharides is complicated by conformational equilibria within their iduronate pyranose rings, the possibilities in phase space are limited because only two conformations, $^1C_4$ chair and $^2S_0$ skewed boat, are energetically favourable [11,13]. This flexibility within α-L-idopyranosyluronate residues might contribute to unique heparin binding properties, thereby affording additional versatility and biological activity. Glycosaminoglycans with approximately the same molecular mass and degree of sulphation but containing the more rigid β-glucopyranosyluronate residues show considerably less biological activity.

Previous findings suggest that different growth factors (and other proteins) might bind to heparin or heparan sulphate in a differential and specific manner. Fibroblast growth factor 1 (FGF-1) binds to two consecutive -IdoA(2-OSO_3)-GlcNSO_3(6-OSO_3) disaccharide units [14]. FGF-2 binds avidly to a heparin hexasaccharide composed of three consecutive → 4)-α-L-IdoA*p*2S(1 → 4)-α-D-GlcN*p*S6S(1 → disaccharide units (i.e. the predominant 'building block' in heparin) [15,16]. However, binding studies involving either chemically modified heparin or native heparan sulphate preparations suggest that whereas the glucosamine *N*-sulphate and the iduronate 2-*O*-sulphate are essential for both FGF-1 and FGF-2 interaction, the glucosamine 6-*O*-sulphates are redundant [14,16–18]. In fact, a search for a minimally *O*-sulphated, yet FGF-2-binding, oligosaccharide implicated a pentasaccharide sequence containing a single iduronate 2-*O*-sulphate in a defined position [16]. Recently, FGF-2 has been co-crystallized with a heparin-derived tetrasaccharide and hexasaccharide containing internal -IdoA(2-SO_3)-GlcNSO_3(6-OSO_3) sequences [19]. The X-ray crystal structure shows the interacting IdoA(2-SO_3) in a $^1C_4$ chair conformation and the interacting GlcNSO_3(6-OSO_3) residue in the $^4C_1$ chair form. Both the 2-*O*-sulphate and 2-*N*-sulphate form tight salt bridges

Abbreviations used: 1D and 2D, one- and two-dimensional; ESFF, electrostatic force field; FGF, fibroblast growth factor; *g*, *gauche*; HETCOR, heteronuclear correlated two-dimensional NMR; IdoA, iduronic acid; IRMA, iterative relaxation matrix approach; MD, molecular dynamics; NOE, nuclear Overhauser effect; RMS, root mean square; *t*, *trans*.

‡ To whom correspondence should be addressed.

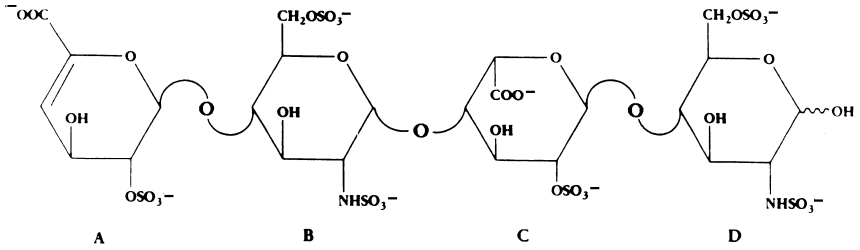

Figure 1 Chemical structure of heparin-derived tetrasaccharide

Residues are labelled as A, B, C and D for uronate, glucosamine, iduronate and glucosamine rings respectively, as discussed in the text. Note that ring A uronate has an unnatural double bond resulting from heparinase digestion.

to basic residues in FGF-2. Thus most of the *O*-sulphate groups in native heparin neither contribute to nor interfere with FGF-2 binding. In contrast, binding of hepatocyte growth factor to heparin/heparan sulphate seems to depend primarily on glucosamine 6-*O*-sulphate groups [20]. The conformation of methylene-*O*-sulphate groups is therefore of interest in understanding heparin–protein interactions involving the sulphate group at this position.

The present study is aimed at determining the solution conformation of the heparin derived tetrasaccharide by using ^{1}H-NMR NOEs and coupling constants, ^{13}C spin–lattice (T_1) relaxation rates, the iterative relaxation matrix approach (IRMA) and restrained molecular dynamics (MD) and energy minimization.

MATERIALS AND METHODS

Heparin tetrasaccharide isolation

Approx. 200 mg of heparin was dissolved in 10 ml of distilled water and dialysed exhaustively, freeze-dried, and prepared at exactly 20 mg/ml in distilled water [21]. To 10 ml of this 20 mg/ml heparin was added 1 ml of sodium phosphate buffer (100 mM sodium phosphate, pH 7, with 200 mM sodium chloride) containing 3 m-i.u. of heparin lyase I (EC 4.2.2.7). The reaction mixture was incubated at 30 °C for 8 h. At reaction completion, the depolymerization mixture was separated and individual low-molecular-mass heparin fractions were isolated by HPLC as discussed previously [6,22].

NMR measurements

For NMR measurements, freeze-dried heparin tetrasaccharide was dissolved to a concentration of 8 mM in ^2H_2O. The pH was adjusted to the desired value by adding microlitre quantities of NaO^2H or ^2HCl to the sample. For most experiments the temperature was controlled at 5 °C to effect shorter relaxation rates and to minimize the contribution from high-energy conformations. ^{13}C-NMR spectra were acquired on Bruker AMX-600 and AM-250 NMR spectrometers operating at ^{13}C frequencies of 150 MHz and 62.5 MHz respectively. ^{1}H-NMR spectra were acquired on a Bruker AMX-600 NMR spectrometer operating at a ^{1}H frequency of 600 MHz.

For ^{1}H resonance assignments, two dimensional (2D) NMR homonuclear Hartman–Hahn spectroscopy spectra, obtained by spin-locking with an MLEV-17 sequence [23] with a mixing time of 60 ms, were used to identify spin systems. NOESY experiments [24,25] were performed for mixing times of 50, 100, 200, 300 and 500 ms to sequentially connect saccharide ring-spin systems and to define NOE build-up curves for use in IRMA calculations described below. ^{1}H–^{1}H coupling constants were derived either from high-resolution 32k one-dimensional (1D) ^{1}H-NMR spectra or from a high-resolution double-quantum-filtered COSY experiment [26,27]. ^{13}C resonance assignments were made via analysis of a ^{13}C–^{1}H heteronuclear correlated 2D NMR (HETCOR) experiment [28] and were consistent with those assignments reported by Merchant et al. [4]. 2D NMR data were acquired in the phase-sensitive mode by using time proportional phase incrementation (TPPI) or States-TPPI [29–31]. The residual water resonance was suppressed by direct irradiation (0.6 s) during the relaxation delay between scans. Spectra were normally collected as 256–512 t_1 experiments each with 2k complex data points and 32–64 scans over a spectral width of 5 kHz in both dimensions with the carrier placed on the water resonance. 2D NMR spectra were processed off-line on an SGI Indigo Extreme workstation with the program Felix® (Biosym/MSI, San Diego, CA, U.S.A.). Free induction decays were generally zero-filled to 2k in the t_1 dimension and the squared sine function apodized before Fourier transformation.

^{13}C spin–lattice relaxation times (T_1) were measured with broadband proton decoupling by using the inversion-recovery method. The number of ^{13}C acquisitions was varied from 10000 to maintain a signal-to-noise ratio in the equilibrium spectrum greater than 10. Ten partly relaxed spectra were acquired for each relaxation experiment. To reduce errors from radio-frequency field inhomogeneities, a composite 180° pulse $[90°_x - 180°_y - 90°_x]$ was used. T_1 values were calculated from the initial slope of relaxation rate curves by using the method described by Daragan and Mayo [32]. To minimize the error in determining these rates, a least-squares method with weighted functions, e.g. $A(t) = \exp(-2W_W t)$, was used [32]. W_W was calculated by minimizing the function $\Sigma_i(I_0 - I_i - A\exp(-W_W t_i))^2$, where I_0 and I_i are equilibrium and transient values respectively of resonance intensities. To calculate the relaxation rate, W, the function:

$$S = S_i\exp(-2W_W t_i)(I_0 - I_i - A\exp(-Wt_i))^2 \quad (1)$$

was minimized. This method reduces errors arising from inaccuracies normally present at the tail of relaxation curves plotted on a semilogarithmic scale. Statistical errors in determining spin–lattice relaxation rates were less than 5%.

For this heparin-derived tetrasaccharide, we are away from the extreme narrowing limit; therefore, ^{13}C T_1 values acquired at two ^{13}C-NMR frequencies were used to calculate a rotational correlation time by using a rigid isotropic model. The root mean square (RMS) value between experimental and theoretical T_1 values was 0.11 for a τ_0 of 400 ps. To account for internal mobility, the Lipari and Szabo [33] model free approach was used and gave a smaller RMS value of 0.05, indicating the

presence of internal motions. From this analysis, motional order parameters, S^2, were derived.

^{1}H spin–lattice relaxation times (T_1) were measured with water suppression by using the inversion recovery method. T_1 values were calculated with the program XSPEC (Bruker Instruments Inc., Billerica, MA, U.S.A., and Spectrospin AG, Zurich, Switzerland).

Full relaxation matrix calculations

NOE build-up rates depend primarily on the frequency of molecular motions and inter-proton distances. For a small isotropically tumbling molecule, the NOE intensity provides relative inter-nuclear distances that can be calibrated by using a known distance. Although heparin-derived tetrasaccharide is rather small (a molecular mass of approx. 1.3 kDa), its high negative charge promotes slower than expected tumbling (rotational correlation time of 0.4 ns). Furthermore the close proximity of intra-ring protons increases the probability of indirect magnetization transfer via other protons (so-called 'spin diffusion'). Analysis of NOE build-up curves at shorter mixing times minimizes the effect of 'spin diffusion'. At the same time, this approach reduces sensitivity and maximizes interference from zero quantum coherences of *J*-coupled protons. Alternatively, NOE cross-peak intensities can be calculated by diagonalization of the complete relaxation matrix for a given structural model and the resulting NOE magnitudes can be compared with experimentally determined values. This latter protocol is known as IRMA [34,35]. The availability of numerous NOE cross-peak intensities obtained with five mixing times (50, 100, 200, 300 and 500 ms) on the tetrasaccharide makes this an attractive approach to derive more accurate inter-proton distance constraints.

IRMA calculations were performed on an SGI Indigo Extreme workstation with different modules in the NMR-Refine program and the electrostatic force field (ESFF) (Biosym/MSI, San Diego, CA, U.S.A.). ^{13}C T_1-derived rotational correlation times were used in IRMA simulations. Relaxation matrix elements were averaged with the NOE mixing time as the weighting function. Initial tetrasaccharide structures were taken from the Brookhaven PDB structural database and modified by introducing a double bond at the C4–C5 position of the non-reducing uronate ring. The total molecular charge was set to 8 (the number of charged groups at pH 6) and partial charges were calculated with the same software. After calculating a set of constraints for each structure, restricted molecular dynamics simulations were run for 5000 ps at 300 K with the dielectric constant, ϵ, set to 6. This was then followed by energy minimization. Final structures were used for subsequent relaxation matrix calculations.

To measure the quality of IRMA calculations, *R*-factors, which provide a comparison between experimental data and model structures, were used. The definition of the NMR *R*-factor used here is analogous with that used by Gonzales et al. [36]:

$$R = \frac{\sum_{\tau_m}\sum_{i}\omega_i(\tau_m)\,|\,A_i^{\mathrm{theo}}(\tau_m) - A_i^{\mathrm{exp}}(\tau_m)\,|}{\sum_{\tau_m}\sum_{i}\omega_i(\tau_m)\,|\,A_i^{\mathrm{exp}}(\tau_m)\,|} \qquad (2)$$

where A_i are cross-peak intensities and ω_i are weighting functions that were chosen to be equal to the mixing time.

RESULTS

^{1}H and ^{13}C-NMR spectra for heparin-derived tetrasaccharide have been previously assigned [6] based primarily on chemical shifts taken from COSY [7] and HETCOR [8] experiments. Of the four sugar rings, namely A, B, C and D from the non-reducing to reducing ends respectively (see Figure 1), glucosamine B and D rings could not be assigned unambiguously. In the present study, sequence-specific resonance assignments have been made by identifying inter-residue H1–H4 NOE connectivities in NOESY spectra (results not shown). Various ring and side-chain conformations discussed in this text are depicted in Figure 2 for clarity.

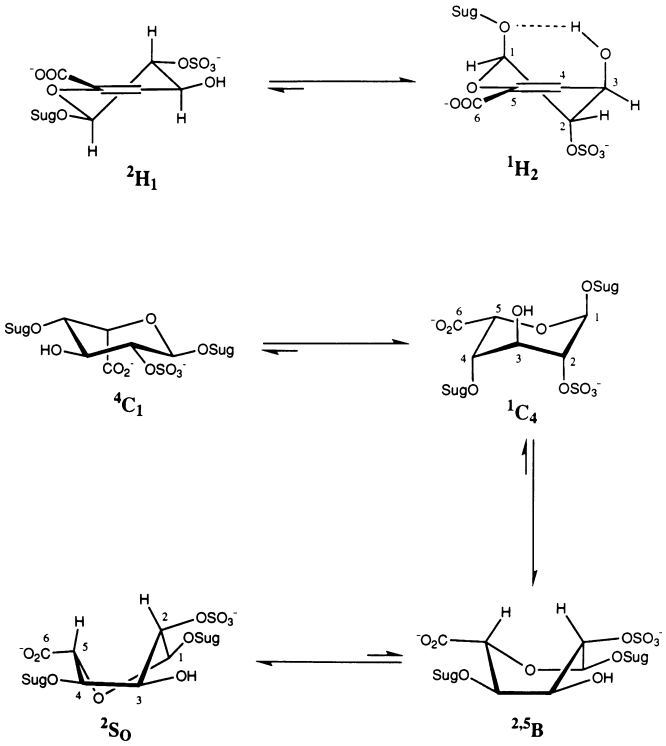

Figure 2 Possible conformations of both uronate (ring A) and iduronate (ring C) residues in the tetrasaccharide

The uronate residue at the non-reducing terminus in the half-chair $^2H_1$ conformer, despite having all substituents equatorial, is less favoured than the $^1H_2$ conformer owing to anomeric, intramolecular hydrogen bonding and allylic effects. The internal iduronate residue can adopt a number of conformations including $^4C_1$, $^1C_4$, $^{2,5}B$ and $^2S_0$. The $^2S_0$ conformer is observed in solution, in which the substitutents are either equatorial or bowsprit and the H2–H5 flagpole interaction is reduced in comparison with that observed in the $^{2,5}B$ conformer.

For structural calculations, comparisons and general discussion, initial heparin tetrasaccharide structures were taken from the heparin dodecasaccharide structure given by Mulloy et al. [37]; a carbon–carbon double bond was added at C4–C5, and for various combinations and permutations of A ring ($^2H_1$ and $^1H_2$) and C ring ($^1C_4$ and $^2S_0$) forms, the tetrasaccharide structure was energy minimized as described in the Materials and methods section. The resulting dihedral angles for all ring forms are listed in Table 1.

Ring conformation of glucosamine residues

Coupling constants obtained from an analysis of 1D ^{1}H-NMR and 2D double-quantum-filtered COSY spectra of the tetrasaccharide indicate that both 2-amino-deoxy-di-2,6-sulpho-α-D-glucosamine (referred to here simply as glucosamine) residues B and D are in the $^4C_1$ conformation (see Figure 2) as suggested for glucosamine residues found in heparin and in other heparin-derived oligosaccharides [11,12,38,39]. The small H1 and H2

Table 1 Dihedral angles from calculated structures and from experimental coupling constants

Dihedral angles are given in degrees. Tetrasaccharide structures have been calculated by energy minimization with an initial sequence derived from a heparin dodecasaccharide [37] and placing a carbon–carbon double bond at C4–C5 as in the heparin lyase-derived tetrasaccharide. Regions for allowed dihedral angles are derived by using the Karplus relation [40] and experimentally determined *J*-coupling constants. Exp., experimental values ± S.E.M.

	A ring			B ring		C ring			D ring	
Dihedral angle	$^1H_2$	$^2H_1$	Exp.	$^4C_1$	Exp.	$^1C_4$	$^2S_0$	Exp.	$^4C_1$	Exp.
H1–C1–C2–H2	63	−177	59 ± 20	59	61 ± 12	71	177	61 ± 10 108 ± 10	56	60 ± 12
H2–C2–C3–H3	−80	−163	−89 ± 20	−179	−152 ± 17	−69	−145	−40 ± 10 −127 ± 10	−175	−152 ± 17
H3–C3–C4–H4	46	63	—*	172	147 ± 16	73	89	57 ± 10 113 ± 10	170	147 ± 16
H4–C4–C5–H5			—	−175	−144 ± 16	51	65	64 ± 11	−174	−144 ± 16

* Coupling constant or theoretical dependence is not available.

coupling constants ($^3J_{1,2} = 3.3$ Hz) indicate an axial–equatorial relationship between H1 and H2 protons, and larger $^3J_{i,j}$ values (more than 8 Hz) for H3, H4 and H5 indicate a *trans*-diaxial relationship between these protons. Use of these *J* values in the Karplus equation [40] yields dihedral angles listed in Table 1. These experimentally determined angles agree well with those calculated by energy minimization of the tetrasaccharide without using NOE-derived distance constraints (Table 1). Furthermore the $^4C_1$ chair form is supported by NOE-based conformational modelling discussed below. These data indicate that neither the unsaturated uronate nor the iduronate residue substantially modifies either glucosamine ring conformation. This conclusion supports a previous observation that adjacent β-D-glucuronate and 2-*O*-sulphated α-L-iduronate residues in a pentasaccharide that corresponds to the ATIII binding site in heparin and contains a 2-amino-2-deoxy-tri-2,3,6-sulpho-α-D-glucopyranose ring [39] do not perturb that glucosamine conformation either.

Ring conformation of uronate residues

The conformation and flexibility of uronate residues in heparin have been the subject of a number of studies [11,13,39,41,42]. The heparin-derived tetrasaccharide under study here contains two different types of uronate residue, a presumably more rigid, 4,5-unsaturated uronate (ring A) at the non-reducing end and a more flexible, 2-*O*-sulphated α-L-idopyranosyluronate (ring C). In solution, the unsaturated uronate ring A with co-planar C3, C4, C5 and O5 atoms can exist in two different half-chair conformations, $^2H_1$ and $^1H_2$ (Figure 2), differentiated by above- and below-plane positions for C1 and C2 atoms. The $^1H_2$ conformer is generally favoured owing to an anomeric effect with ring B glucosamine, a potential hydrogen bond between O1 and HO3, and an allylic effect at C3 (see Figure 2). The $^2H_1$ conformer, with C1 and C2 lying below and above this plane respectively, shows $^3J_{1,2}$ and $^3J_{2,3}$ coupling constants greater than 6 Hz, whereas the $^1H_2$ conformation, with C2 and C1 lying below and above this plane respectively, shows smaller and near-equal $^3J_{1,2}$ and $^3J_{2,3}$ coupling constants of less than 4 Hz. Initial heparin tetrasaccharide structures were taken from the heparin dodecasaccharide structure given by Mulloy et al. [37]; a carbon–carbon double bond was added at C4–C5, and with the A ring in the $^2H_1$ or $^1H_2$ form the tetrasaccharide structure was energy minimized as described in the Materials and methods Section. The resulting dihedral angles for both forms are listed in Table 1. Experimentally, $^3J_{1,2}$ and $^3J_{2,3}$ values for ring A are 2.0 and 1.0 Hz respectively, and by using the Karplus equation [40], H1–C1–C2–H2 and H2–C2–C3–H3 torsion angles are estimated to be +59° and −89° respectively (Table 1), consistent with a preferred $^1H_2$ half-chair conformation.

For the 2-*O*-sulpho-α-L-idopyranosyluronate (called simply iduronate) ring C, $^3J_{2,3}$ and $^3J_{3,4}$ coupling constants are 6.6 and 3.8 Hz respectively, with assessable dihedral angles H2–C2–C3–H3 and H3–C3–C4–H4 [40] listed in Table 1. The H2–C2–C3–H3 dihedral angle deviates considerably from that expected for a $^1C_4$ chair form, which should give $^3J_{2,3}$ and $^3J_{3,4}$ both less than 5 Hz. For the most part, the calculated dihedral angles in fact suggest that the average solution conformation for the iduronate ring C is a slightly twisted boat form, $^2S_0$ (Table 1). (Four possible conformers for ring C, i.e. $^4C_1$, $^1C_4$, $^{2,5}B$ and $^2S_0$ forms, are shown in equilibrium in Figure 2.) This conclusion is further supported by variable-mixing-time NOESY data and IRMA NOE-build-up curve simulations (see below). Furthermore NOESY spectra show intra-residue NOE cross-peaks between H2 and H5 and between H1 and H3 in ring C, which would not be observed in a true $^1C_4$ chair form. However, in a $^{2,5}B$ boat or $^2S_0$ twisted boat form, these NOEs might be observed. Either of these conformations tends to minimize unfavourable 1,3 diaxial non-bonded interactions that are expected in the $^1C_4$ chair form where four of the substituents occupy axial positions and only the carboxy group is equatorial. In this respect, the conformation of ring C becomes a boat, bringing three of the substituents into equatorial (e) positions and the 2-*O*-sulphate and carboxy group in the bowsprit (bs) orientation. The H2 and H5 flagpole (fp) protons are pulled apart resulting in a $^2S_0$ twist-boat in which the fp–fp interaction is minimized and the conformation becomes more stable (see Figure 2). One exception to this reasoning can be found in the difference between calculated and experimentally determined H1–C1–C2–H2 dihedral angles (Table 1). The two possible ranges for this angle derived from the coupling constant by using the Karplus equation are far from the calculated value given in Table 1 for the $^2S_0$ form. By the IRMA procedure, however, this dihedral angle in the modelled conformation is considerably closer to the experimentally determined value.

Orientation of 6-*O*-sulphate side-chains

The orientation of both hydroxymethyl and 6-*O*-sulphate is determined by rotation about the C5–C6 bond with dihedral angle ω (O5–C5–C6–O6). Normally, this orientation is described by three staggered conformations [*gauche* (*g*) or *trans* (*t*)]: *gg*, *gt*,

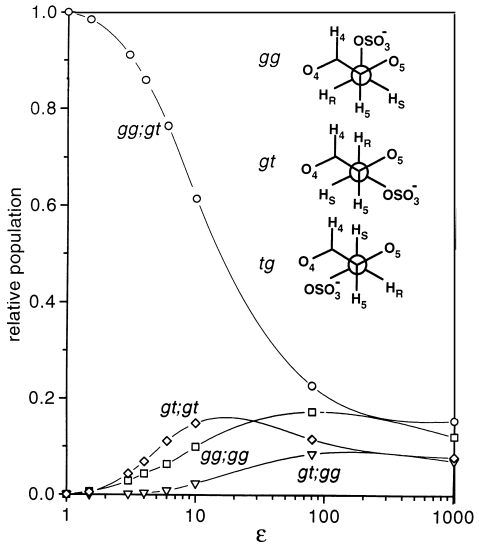

Figure 3 Dependence of 6-*O*-sulphate side-chain orientations on the dielectric constant

While maintaining the A and C rings in the $^1H_2$ and $^2S_0$ forms respectively and the B and D rings in $^4C_1$ chair conformations, 6-*O*-sulphate side-chain rotomer populations were calculated as a function of the dielectric constant. Various side-chain conformations are depicted, showing possible orientations as discussed in the text.

Table 2 *R*-factors

R-factors were calculated with eqn. (2) for all mixing times using either all or only inter-residue NOEs (in parentheses).

	Initial conformation of C ring			
	$^1C_4$		$^2S_0$	
	Initial orientation of B ring 6-*O*-sulphate		Initial orientation of B ring 6-*O*-sulphate	
IRMA iteration	*gg*	*gt*	*gg*	*gt*
1	0.48 (0.30)	0.46 (0.50)	0.49 (0.34)	0.52 (0.46)
2	0.41 (0.37)	0.39 (0.21)	0.40 (0.19)	0.40 (0.18)
3	0.42 (0.36)	0.37 (0.15)	0.40 (0.17)	0.40 (0.19)

tg [43] as shown in the inset to Figure 3. X-ray, optical and NMR studies indicate that the major contribution to differences in monosaccharide conformational populations is the relative orientation of the hydroxymethyl group (or 6-*O*-sulphate group) and the substituent at the adjacent C4 position. For glucomonosaccharides, the ratio *gg*:*gt*:*tg* is 6:4:0 [44]. However, this ratio can vary with solvent conditions, steric interactions, electrostatics and hydrogen bonding [43]. Orientational preferences for the C6-*O*-sulphated sugar side-chains can be obtained by using coupling constants between H5 and the two H6 protons, i.e. $^3J_{5,6R}$ and $^3J_{5,6S}$, provided that stereospecific assignments for $H6_R$ and $H6_S$ are known or can be surmised. This latter point is crucial to discriminate between *gt* and *tg* rotomers. Unfortunately, tetrasaccharide $^3J_{5,6}$ coupling constants could not be measured accurately for all four 6-*O*-sulphate group protons. Qualitatively, for ring D, a larger coupling constant was observed for the more downfield-shifted 6H proton resonance, suggesting predominance of either the *gt* or *tg* rotomer. For ring B, however, approximately equal coupling constants were found for both 6H resonances, suggesting a major contribution from the *gg* rotomer.

Stereospecific H6 methylene proton assignments have been made in monosaccharides by using partly deuterated hydroxymethyl groups [45]. For longer-chain heparin molecules, Mulloy et al. [37] accepted these same relative hydroxymethyl *R* and *S* proton chemical shifts and concluded a preferred *gg* conformation for 6-*O*-sulphated side-chains. Because it is unclear whether or not this assumption is correct for polysulphated oligosaccharides, we calculated the internal energy of the tetrasaccharide in different conformations by using an electrostatic force field (ESFF in DISCOVER) and partial charges (see the Materials and methods section). Electrostatic interactions were not explicitly considered by Mulloy et al. [37]. During our calculations the terminal A ring and non-terminal C ring were fixed in their preferred conformations $^1H_2$ and $^2S_0$ respectively, with B and D rings having all nine possible 6-*O*-sulphate group conformations: *gg*,*gg*; *gg*,*gt*; *gg*,*tg*, etc. Each overall conformation was minimized by using different values for the dielectric constant, ϵ, to provide more reliable results. The dependence of relative rotomer populations on ϵ is shown in Figure 3. For ϵ in the range 4–10, *gg* and *gt* (or *tg*) 6-*O*-sulphate side-chain orientations in the B ring and a *gt* orientation in the D ring contribute most to the ensemble of sampled conformations. For ring D, this result agrees qualitatively with the ratio for hydroxymethyl rotomer populations mentioned above and is consistent with our qualitative *J* values. On the basis of these coupling constants and internal energy calculations, we have assigned for ring D the more downfield H6 signal to the $H6_R$ proton and the more upfield resonance to the $H6_S$ proton. This is just the opposite of glucose hydroxymethyl assignments [45].

Motional dynamics

^{13}C spin–lattice (T_1) relaxation rates for carbons in the tetrasaccharide were measured at two resonance frequencies (62.5 and 150 MHz) to determine the overall rotational correlation time and motional order parameters, S^2. Only small differences in T_1 values were observed among different carbon positions in all four rings. At 62.5 MHz, T_1 values ranged from 0.13 to 0.18 s. These differences most probably originate from variations in internal motions. Ring-averaged motional order parameters [33], S^2, all fell in the range 0.83 ± 0.05 to 0.98 ± 0.02. S^2 values are largest for residues B (0.98 ± 0.02) and C (0.97 ± 0.03) and are smallest for residues A (0.87 ± 0.03) and D (0.83 ± 0.05) (all values given $\pm$S.E.M.). As expected, these order parameters indicate decreased internal motions in rings B and C relative to the terminal rings A and D. Given the generally large S^2 values, however, overall inter-ring mobility is highly constrained. In this respect a simple rigid isotropic rotational model was used in subsequent IRMA calculations. This isotropic hard-sphere rotational model with a rotational correlational time of 400 ps can account fairly accurately for observed T_1 values. Alternatively, anisotropic tumbling over a restricted range of angles between CH vectors and the main symmetrical top axis (as was found for longer oligosaccharides [37]) can also account for observed T_1 values. This alternative explanation is less likely for the tetrasaccharide studied here because components of the moment of inertia tensor are nearly the same and multiple charged groups promote greater isotropic tumbling.

NOE-based conformational modelling

Four different initial structures were used in IRMA calculations. Because the non-terminal iduronate residue C can exist in two

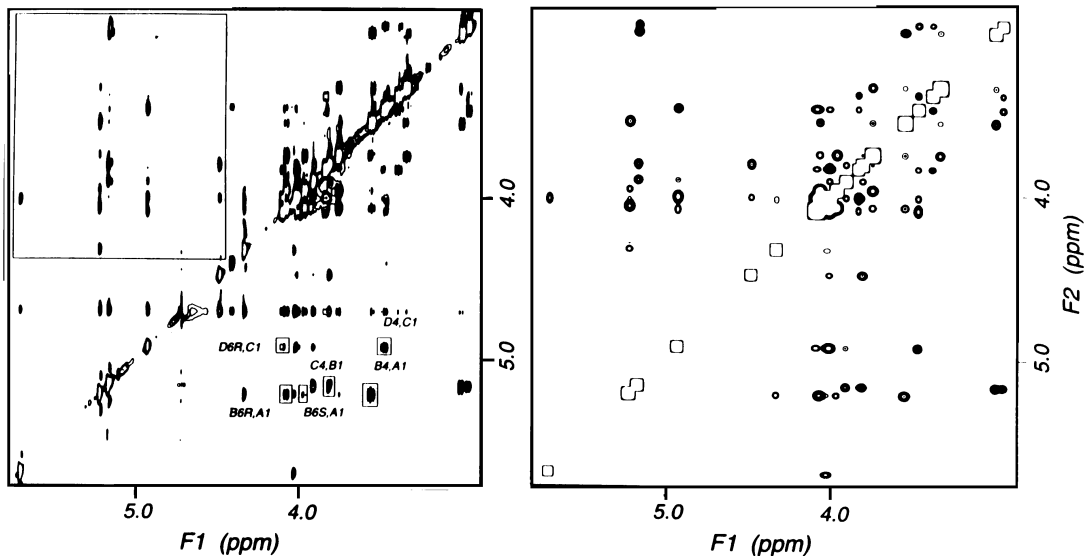

Figure 4 Tetrasaccharide NOESY spectra

Two NOESY spectra are shown for the tetrasaccharide. Left panel, experimental ^{1}H NOESY data accumulated at 600 MHz with a mixing time of 500 ms. Right panel, an IRMA-calculated ^{1}H NOESY spectrum of the same spectral region. The residual water resonance is absent from the calculated spectrum.

forms, $^1C_4$ and $^2S_0$, both forms were used as initial structures and, for reasons outlined above, both *gg* and *gt* 6-*O*-sulphate side-chain rotomers in residue B were used in separate calculations with the glucosamine D ring 6-*O*-sulphate group being initially set in the *gt* rotomer state. Furthermore owing to the absence of a $^3J_{NH,CH2}$ coupling constant (NH proton exchanged with deuteron ^{2}H), the H2–C2–N–H dihedral angle was fixed in the *trans* state according to Mulloy et al. [37].

Symmetry-related NOESY cross-peaks were volume integrated and averaged. Some NOESY cross-peaks were not used owing to NOE build-up curve anomalies arising from cross-peaks close to the diagonal. A total of 37 NOEs measured at five mixing times were used as input for IRMA calculations. Four NOEs, B2–B4, B3–B5, D2–D4 and D3–D5, were taken as references for calculating relaxation matrix elements. With rings B and D in a $^4C_1$ conformation, these inter-proton NOEs provide good distance calibrations. The resulting structures were then used in a 5000 ps NOE-restrained molecular dynamics simulation at 300 K with a force constant of 20 kcal/mol/Å^2 and $\epsilon = 6$. Dihedral angular constraints obtained from experimental J coupling constants were not included in these simulations. Structures were then energy minimized and used as initial structures in subsequent IRMA calculations.

R-factors given in Table 2 indicate that three iterations of this protocol are sufficient for convergence of the IRMA procedure. Figure 4 compares an actual and a calculated NOESY spectrum. Apart from the residual water resonance observed in the experimental NOESY data set, the calculated NOESY spectrum yields very similar cross-peak patterns. For a better comparison of NOE amplitudes, Figure 5 shows the respective stacked plots

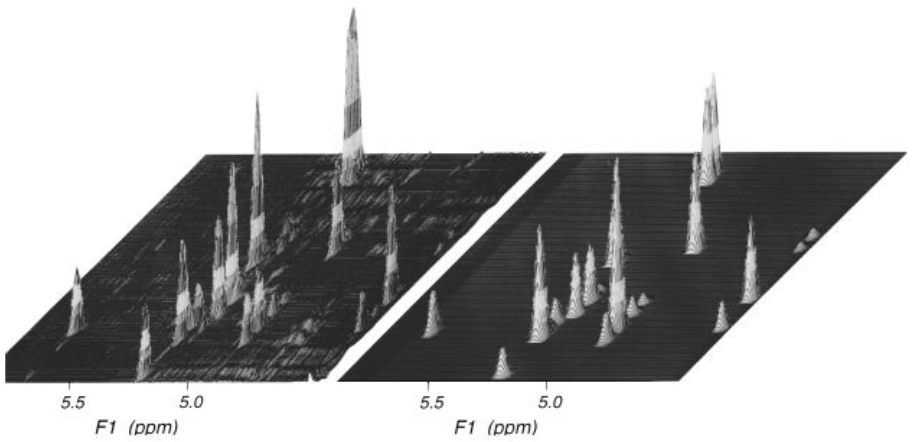

Figure 5 Tetrasaccharide NOESY spectra in stacked-plot format

Regions from two NOESY spectra (experimental at the left and IRMA calculated at the right) are shown in stacked-plot format.

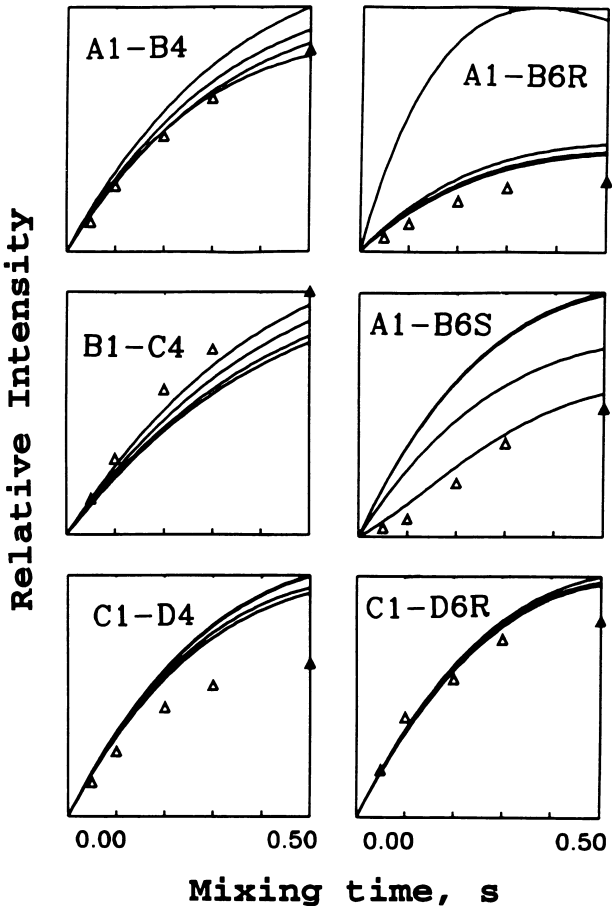

Figure 6 NOE build-up curves

Experimental and IRMA-calculated NOE build-up curves are shown for several inter-proton NOEs as indicated in the figure. Triangles represent experimentally determined NOEs and lines give calculated build-up curves for four final structures calculated with the modelling protocol described in the text.

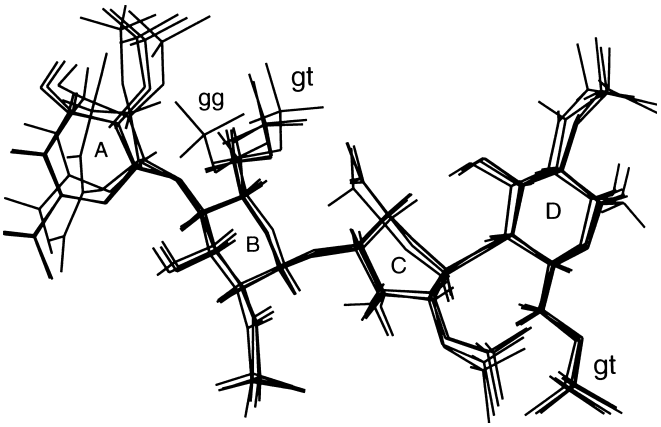

Figure 7 Tetrasaccharide structures

Four final IRMA-calculated structures with the modelling protocol described in the text have had their rings B, C, and D superimposed. Three of the four structures have the B ring 6-*O*-sulphate side chain as the *gt* conformer, whereas one shows the *gg* conformer. The D ring side chain has all four in the *gt* conformer state.

Table 3 Glycosidic bond dihedral angles

	Dihedral angle			
	ϕ (deg)		ψ (deg)	
Glycosidic linkage	Solution*	Crystal†	Solution*	Crystal†
A–B	45 ± 6	42	13 ± 4	18
B–C	−43 ± 2	−18	−42 ± 1	−3
C–D	45 ± 1	57	15 ± 1	25

* Average over four IRMA structures; values given ± S.E.M..
† ϕ,ψ angles taken from [19].

from the same experimental and calculated NOESY data sets. Although amplitudes vary somewhat, it should be emphasized that NOEs are heavily weighted by an inverse sixth power of the inter-nuclear distance; therefore even a factor 2 change in amplitude (assuming that motional effects have been treated equally) will affect the inter-nuclear distance by only a few tenths of an ångström. Figure 6 presents some typical NOE build-up curves; triangles indicate experimental data and lines indicate IRMA-calculated curves for four final tetrasaccharide structures, which have been superimposed in Figure 7. Although the fits do not always seem to account for observed NOE intensities accurately, the resulting distance variations are minimal, being on the order of 0.1–0.2 Å. The set of glycosidic bond dihedral angles given in Table 3 that define the overall conformation of the tetrasaccharide (Figure 7) results from computational analysis of experimentally determined intra- and inter-ring NOE build-up curves, IRMA calculations and restrained molecular dynamics simulations with an ESFF. Experimental data always bias conformational modelling results when strong force constants are used for NOE-derived distance constraints. For these tetrasaccharide structures, however, it was found that glycosidic bond rotational energy profiles are rather steep (results not shown) and the dependence of dihedral angles on the force constant is minimal. RMS deviation (RMSD) values for these tetrasaccharide structures are less than 0.2 Å for all ring atoms in residues B, C and D. RMSD values for A ring and side-chain atoms are slightly higher, at about 1 Å.

The absence of significant distance violations supports our initial use of the chair conformation for both glucosamine rings (Table 4) and the D ring 6-*O*-sulphate group being predominantly in the *gt* state (Table 5). NOE distance violations for the B ring 6-*O*-sulphate group in the *gg* conformation (Table 5) indicate the presence of mostly the *gt* form with some *gg* character. In agreement with our previous conclusions, iduronate residue C has a slightly twisted boat form due to the presence of an H2–H5 NOE that provides a relatively strong non-bonded potential to overcome the chair–boat energy barrier. Furthermore minor variations in ring NOEs (Table 4) might indicate some contribution from the $^1C_4$ form in ring C. On the basis of coupling constants, $^1H_2$ is the major ring conformation for uronate residue A. After restrained MD runs, however, the $^1H_2$ form became distorted (Table 4) owing to an NOE constraint between A1 and A3. Because the A1–A3 inter-proton distance is one-sixteenth as long in the $^2H_1$ form, a minor fraction of $^2H_1$ is most probably

Table 4 Distance violations for IRMA structures: rings, no side chains

Only violations more than 0.1 Å are listed. Exp., experimental values ± S.E.M.

A ring*				B ring			C ring			
Proton pair	$^1H_2$	$^2H_1$	Exp.	Proton pair	$^4C_1$	Exp.	Proton pair	$^2S_0$	$^1C_4$	Exp.
1–2	2.52	3.07	2.75 ± 0.04	4–5	2.95	2.60 ± 0.05	1–2	2.92		2.67 ± 0.07
2–3	2.63	3.08	2.89 ± 0.14				2–3	2.95		2.55 ± 0.20
3–4	2.45	2.56	2.84 ± 0.02				2–5	2.97		3.20 ± 0.11
1–3	4.3	2.7	3.32 ± 0.24							

* From structures energy-minimized without constraints.

Table 5 Distance violations for IRMA structures: side chains

Only violations more than 0.1 Å are listed. Exp., experimental values ± S.E.M. N/A, not applicable.

	5–6*R*	Exp.	5–6*S*	Exp.	4–6*R*	Exp.	4–6*S*	Exp.	1–6*R*	Exp.	1–6*S*	Exp.
B ring												
gg	2.45		2.35		2.97		3.68		1.94		3.51	
		2.14 ± 0.04		2.22 ± 0.02		2.78 ± 0.08		3.20 ± 0.06		2.40 ± 0.05		3.04 ± 0.17
gt	3.02		2.29		2.64		3.42		2.41		2.83	
D ring												
gt	2.90	2.44 ± 0.03	2.33	2.22 ± 0.05	2.35	2.59 ± 0.13	2.86	2.55 ± 0.08	2.79	2.14 ± 0.04	N/A	

present in equilibrium with the major $^1H_2$ form. IRMA calculations do not discriminate well between these two conformations. Lastly, no 6-*O*-sulphate oxygens were found within 4 Å of any potential hydrogen-bond donor (2.5 Å being the standard O–H H-bond distance), thereby ruling out the possible influence of hydrogen-bonding in determining the observed conformations.

DISCUSSION

The use of a homogeneous fraction of heparin-derived tetrasaccharide allows one to determine a number of reliable experimental conformational parameters essential for understanding and modelling the structure of longer heparin chains. Tetrasaccharide ring conformations show both glucosamine residues B and D in the $^4C_1$ conformation as proposed for this residue in parent heparin and in other heparin-derived oligosaccharides [11,12,38,39]. Moreover neither uronate (ring A) nor iduronate (ring C) substantially modifies this glucosamine ring conformation, supporting a previous observation that adjacent β-D-glucuronate and 2-*O*-sulphated α-L-iduronate residues in the synthetic ATIII binding-site pentasaccharide do not perturb its glucosamine ring conformation [39]. The orientation of the 6-*O*-sulphate group in the D ring was determined as being primarily *gt*. For the B ring the orientation of the 6-*O*-sulphate group is not as clear. Rotational energy profiles and coupling constants suggest mostly *gg* character; however, some NOEs are more consistent with the presence of a *gg*–*gt* rotomer equilibrium. The *gg* character in the orientation of the B ring 6-*O*-sulphate group might result from the presence of the unsaturated uronate ring A instead of the normal iduronate ring as in position C. The existence of *gt* character in the glucosamine ring D is consistent with the results of Nishida et al. [44] for hydroxymethyl rotomer populations in monosaccharides, but runs contrary to the structure given by Mulloy et al. [37] for a heparin dodecasaccharide where the side chains were fixed in the *gg* conformation. In contrast our glucosamine B ring does show the *gg* side-chain orientation. Because the heparin tetrasaccharide is short and the glucosamine D ring is at a terminal position, the *gt* side-chain state might be preferred for a terminal ring.

For residues A and C, the most probable ring conformations are the $^1H_2$ and twisted boat, $^2S_0$ respectively. The twist of the boat in ring C brings three substituents (except for the C2 sulphate and the carboxy group) into equatorial positions, thereby minimizing the unfavourable 1,3 steric interactions, which would be expected for axial positions in the $^1C_4$ chair form. The conformation of iduronate in parent heparin and in dermatan sulphate has been suggested to exist in a slightly distorted (C2 and C3 positions) $^1C_4$ chair conformation [13,39,46]. Huckerby et al. [42], who analysed disaccharides obtained after chemical depolymerization of heparin, also concluded that the iduronate residue is not a true $^1C_4$ chair form. Small deviations in expected coupling constants and NOEs in the tetrasaccharide, however, might indicate a minor contribution from other ring forms that coexist in equilibrium. Conformational equilibria of the α-L-idopyranosyluronate have been found to depend on its substituents as well as on those from adjacent residues [11,13,39,41,42].

Ferro et al. [13] investigated the conformation of α-L-iduronate in various mono- and oligosaccharides and suggested that when α-L-idopyranosyluronate and 2-*O*-sulpho-α-L-idopyranosyluronate residues are present within a saccharide sequence only the $^1C_4$ and $^2S_0$ conformers are present in equilibrium. When 2-*O*-sulphated α-L-idopyranosyluronate is at the non-reducing terminus it exists mainly in the $^1C_4$ form but when it is present at non-terminal positions the $^2S_0$ form is the major contributor to the equilibrium. This equilibrium is shifted heavily to the $^1C_4$ form (more than 90%) for the iduronate monomer (methylglycoside), whereas for iduronate preceded by a 3-*O*-sulphated glucosamine in heparin's ATIII binding site it is shifted more towards the $^2S_0$ form [11,13,39]. This ring distortion to an $^2S_0$

form is considered essential for the high-affinity interaction between heparin and ATIII [11,39] and is thought to be the result of the presence of an adjacent trisulphated glucosamine residue with a 3-*O*-sulphate group. In the absence of structural data it is impossible to establish whether the 3-*O*-sulphate group does indeed distort the conformation of the adjacent iduronate. The tetrasaccharide under investigation here does not contain a trisulphated glucosamine adjacent to a 2-*O*-sulphated α-L-iduronate.

The overall conformation of the tetrasaccharide has all sulphates extending equatorially from each ring. The derived glycosidic bond angles give a right-handed sense to the inter-ring conformation. In general this tetrasaccharide structure agrees with the heparin dodecamer structure of Mulloy et al. [37]. However, the dihedral angles in the tetrasaccharide B–C linkage do differ from those calculated for the glucosamine–iduronate disaccharide unit in the longer heparin chain [37] but are close to those values reported for the glucosamine–iduronate disaccharide when the iduronate ring is in the alternative $^1C_4$ chair form as opposed to the $^2S_0$ form found to be preferred in this tetrasaccharide. In the present work, the tetrasaccharide conformation results from experimental NOE build-up curves, IRMA and restrained MD calculations and energy minimization with an electrostatic force field. Although one can bias an experimentally based conformation by using strong force constants for NOE-derived distance constraints, the dependence of dihedral angles on the force constant for these heparin tetrasaccharide structures was found to be minimal. This is supported by the observation of high motional order parameters and rather steep rotational energy profiles for glycosidic bond dihedral angles, which indicate highly constrained inter-ring mobilities.

When this heparin-derived tetrasaccharide was co-crystallized in the presence of FGF-2, the X-ray structure [19] showed that the interacting iduronate residue (ring C) is in a true $^1C_4$ chair form, with all of its substituents, except the C5 carboxylate, axially oriented. The $^1C_4$ chair form of iduronate is apparently stabilized by interactions with basic amino acid residues in FGF-2 because the non-interacting 2-*O*-sulphated α-L-iduronate is not similarly distorted. For the tetrasaccharide in solution, iduronate (ring C) exists primarily in the $^2S_0$ twisted boat form even in the absence of an adjacent 3-*O*-sulphated glucosamine residue. Here the iduronate is flanked by two 2-amino-2-deoxy-di-2,6-sulpho-α-D-glucopyranose residues. A trisaccharide prepared from the tetrasaccharide by removing the unsaturated uronate residue with mercuric acetate [47] shows the same $^3J_{2,3}$ coupling constant (8.5 Hz), indicating that the iduronate residue is indeed twisted at the C2 and C3 bond. The need to consider the $^2S_0$ conformation in order to interpret the unusual iduronate coupling constant was first suggested by Auge and David [48]. The larger iduronate $^3J_{2,3}$ coupling constants observed for both the tetrasaccharide and the trisaccharide suggest that the $^2S_0$ twisted boat form is an important contributor to the conformational equilibrium of all 2-*O*-sulphated α-L-idopyranosyluronate residues in heparin. Furthermore the variability of coupling constants for different α-L-iduronate derivatives described by Ferro et al. [13] may be due to the flexibility of the ring around the skewed boat form rather than to the existence of an equilibrium between two distinct conformations.

Further structural comparison of the solution free and crystal FGF-2 bound tetrasaccharide shows essentially the same B and D ring conformations (average ring atomic RMSD values of 0.07 and 0.11 Å respectively) with both side chains in the *gg* orientation. The slightly higher RMSD value for the D ring might reflect increased internal mobility owing to its terminal position. The crystal structure D ring side chain is distorted ($-12°$ instead of $-60°$). Moreover because the orientation is a *gg* form in the FGF-2 bound structure, this supports the idea that non-terminal, or in this case structure-bound, glucosamine 6-*O*-sulphate side-chain orientations prefer the *gg* state. The average atomic RMSD value for ring A comes out higher at 0.24 Å, most probably because of the equilibrium between $^1H_2$ and $^2H_1$ forms in solution. Glycosidic bond angles are compared in Table 3. The A–B and C–D ring orientations are essentially the same in solution and in the FGF-2 bound state. The B–C ring ϕ,ψ angles, in contrast, each deviate by about 25–30°. This is apparently due to the C ring conformational equilibrium.

Conclusions

The NMR solution conformation of a heparin-derived tetrasaccharide has been derived. As in an FGF-2-bound crystal state, both glucosamine rings exist in the $^4C_1$ chair conformation, and unlike the terminal ring D, the internal ring B 6-*O*-sulphate preferred orientation is *gauche–gauche*. In solution, both uronate and iduronate rings interconvert between twisted boat forms. When the tetrasaccharide is bound to FGF-2, the uronate (ring A) remains in the twisted boat conformation, whereas the energy barrier to the iduronate (ring C) $^1C_4$ chair form is overcome, most probably by electrostatic interactions with basic amino acid residues. Although glycosidic bond angles between the free and bound states do vary between 10° and 30° for rings B–C and C–D (but not A–B), the overall tetrasaccharide conformation is maintained.

This work was supported by grants from the American Heart Association (AHA-96006050 to K.H.M.), the National Science Foundation (MCB-9420203 to K.H.M.) and the National Institutes of Health (GM-38060 to R.J.L.) and benefited from the use of the high-field NMR facility at the University of Minnesota.

REFERENCES

1 Jeanloz, R. W. (1975) Adv. Exp. Med. Biol. **52**, 3–12
2 Lindahl, U. (1974) Int. Rev. Sci., Org. Chem. Ser. **2** (7), 283–289
3 Perlin, A. S., Mackie, D. M. and Dietrich, C. P. (1971) Carbohydr. Res. **18**, 185–192
4 Merchant, Z. M., Kim, Y. S., Rice, K. G. and Linhardt, R. J. (1985) Biochem. J. **229**, 369–377
5 Linker, A. and Hovingh, P. (1984) Carbohydr. Res. **127**, 75–94
6 Pervin, A., Gallo, C., Jandik, K. A., Han, X.-J. and Linhardt, R. J. (1995) Glycobiology **5**, 83–95
7 Gettins, P. and Horne, A. (1992) Carbohydr. Res. **223**, 81–98
8 Horne, A. and Gettings, P. (1992) Carbohydr. Res. **225**, 43–57
9 Ragazzi, M., Ferro, D. R., Provasoli, A., Pumilia, P., Cassinari, A., Torri, G., Guerrini, M., Casu, B., Nader, H. B. and Dietrich, C. P. (1993) J. Carbohydr. Chem. **12**, 523–535
10 Gould, S. E. B., Gould, R. O., Rees, D. A. and Wight, A. W. (1975) J. Chem. Soc. Perkin Trans. II, 392
11 Ferro, D. R., Provasolli, A., Ragazzi, M., Torri, G., Casu, B., Gatti, G., Jacquinet, J. C., Sinay, P., Petitou, M. and Choay, J. (1986) J. Am. Chem. Soc. **108**, 6773–6778
12 Desai, U. R., Wang, H. M., Kelly, T. R. and Linhardt, R. J. (1993) Carbohydr. Res. **241**, 249–259
13 Ferro, D. R., Provasolli, A., Ragazzi, M., Casu, B., Torri, G., Bossennec, V., Perty, B., Sinay, P., Petitou, M. and Choay, J. (1990) Carbohydr. Res. **195**, 157–167
14 Mach, H., Volkin, D. B., Burke, C. J., Middaugh, C. R., Linhardt, R. J., Fromm, J. R. and Loganathan, D. (1993) Biochemistry **32**, 5480–5489
15 Tyrrell, D. J., Ishihara, M., Rao, N., Horne, A., Kiefer, M. C., Stauber, G. B., Lam, L. H. and Stack, R. J. (1993) J. Biol. Chem. **268**, 4684–4689
16 Maccarana, M., Casu, B. and Lindahl, U. (1993) J. Biol. Chem. **268**, 23898–23905
17 Habuchi, H., Suzuki, S., Saito, T., Tamura, T., Harada, T., Yoshida, K. and Kimata, K. (1992) Biochem. J. **285**, 805–813
18 Turnbull, J. E., Fernig, D. G., Ke, Y., Wilkinson, M. C. and Gallagher, J. T. (1992) J. Biol. Chem. **267**, 10337–10341
19 Fahem, S., Hileman, R. E., Fromm, J. R., Linhardt, R. J. and Rees, D. C. (1996) Science **271**, 1116–1120

20 Lyon, M., Deakin, J. A., Mizuno, K., Nakamura, T. and Gallagher, J. T. (1994) J. Biol. Chem. **269**, 11216–11223
21 Linhardt, R. J., Rice, K. G., Kim, Y. S., Lohse, D. L., Wang, H. M. and Loganathan, D. (1988) Biochem. J. **254**, 781–787
22 Loganathan, D., Wang, H. M., Mallis, L. M. and Linhardt, R. J. (1990) Biochemistry **29**, 4362–4368
23 Bax, A. and Davis, D. G. (1985) J. Magn. Reson. **65**, 355–360
24 Jeener, J., Meier, B., Backman, P. and Ernst, R. R. (1979) J. Chem. Phys. **71**, 4546–4550
25 Wider, G., Macura, S., Anil-Kumar, Ernst, R. R. and Wüthrich, K. (1984) J. Magn. Reson. **56**, 207–234
26 Piantini, U., Sørensen, O. W. and Ernst, R. R. (1982) J. Am. Chem. Soc. **104**, 6800–6805
27 Shaka, A. J. and Freeman, R. (1983) J. Magn. Reson. **51**, 161–169
28 Bax, A., Griffey, R. H. and Hawkins, B. L. (1983) J. Magn. Reson. **55**, 301–308
29 States, D. J., Haberkorn, R. A. and Ruben, D. J. (1982) J. Magn. Reson. **48**, 286–293
30 Marion, D. and Wüthrich, K. (1983) Biochem. Biophys. Res. Commun. **113**, 967–975
31 Wüthrich, K. (1986) NMR of Proteins and Nucleic Acids, Wiley-Interscience, New York
32 Daragan, V. A. and Mayo, K. H. (1993) Biochemistry **32**, 11488–11499
33 Lipari, G. and Szabo, A. (1982) J. Am. Chem. Soc. **104**, 4546–4559
34 Boelens, R., Koning, T. M. G. and Kaptein, R., (1988) J. Mol. Struct. **173**, 299–311
35 Boelens, R., Koning, T. M. G., van der Marel, G. A., van Boom, J. H. and Kaptein, R. (1989) J. Magn. Reson. **82**, 290–308
36 Gonzales, C., Rullmann, J. A. C., Bonvin, A. M. J. J., Boelens, R. and Kaptein, R. (1991) J. Magn. Reson. **91**, 659–664
37 Mulloy, B., Forster, M. J., Jones, C. and Davies, D. B. (1993) Biochem. J. **293**, 849–857
38 Casu, B., (1985) Adv. Carbohydr. Chem. Biochem. **43**, 51–60
39 Torri, G., Casu, B., Gatti, G., Petitou, M., Choay, J., Jacquine, J. C. and Sinay, P. (1985) Biochem. Biophys. Res. Commun. **128**, 134–140
40 Karplus, M. (1963) J. Am. Chem. Soc. **85**, 2870–2871
41 Huckerby, N. T. and Nieduszynski, A. I. (1982) Carbohydr. Res. **103**, 141–145
42 Huckerby, N. T., Senderson, P. N. and Nieduszynski, A. I. (1985) Carbohydr. Res. **138**, 199–206
43 Bock, K. and Duus, J. O. (1994) J. Carbohydr. Chem. **13**, 513–543
44 Nishida, J., Hori, H., Ohrui, H. and Meguro, H. (1988) J. Carbohydr. Chem. **7**, 239–250
45 Hori, H., Nakazima, T., Nishida, Y., Ohrui, H. and Meguro, H. (1986) J. Carbohydr. Chem. **5**, 585–594
46 Gatti, G., Casu, B., Torri, G. and Vercellotti, J. R. (1979) Carbohydr. Res. **68**, C3–C7
47 Ludwigs, U., Elgavis, A., Esko, J. D., Meezan, E. and Roden, L. (1987) Biochem. J. **245**, 795–804
48 Auge, J. and David, S. (1984) Tetrahedron **40**, 2101–2106

Received 29 February 1996/18 April 1996; accepted 23 April 1996